DFB fiber laser sensor for simultaneous measurement of acoustic and magnetic fields

Rui Ma (马 瑞)[1,2], Wentao Zhang (张文涛)[1,2,*], Wenzhu Huang (黄稳柱)[1,2], and Fang Li (李 芳)[1,2]

[1]*State Key Laboratory of Transducer Technology, Institute of Semiconductors, Chinese Academy of Sciences, Beijing 100083, China*

[2]*College of Materials Science and Opto-Electronic Technology, University of Chinese Academy of Sciences, Beijing 100049, China*

*Corresponding author: zhangwt@semi.ac.cn

A novel distributed feedback (DFB) fiber laser sensor, which can measure acoustic and magnetic fields simultaneously, is proposed. The magnetic field can be measured by detecting the change of resonant frequency of the fiber laser, and the acoustic pressure can be measured by detecting the phase shift of the fiber laser. Both of the signals can be simultaneously demodulated in the frequency domain without affecting each other. Experimental studies show that the acoustic pressure sensitivity of this sensor is about -130 dB (0 dB re 1 pm/μPa) and the sensor has a good linearity with a magnetic field sensitivity of 0.57 Hz/mT.

OCIS codes: 060.2310, 060.2370, 060.3510, 230.3810.
doi: 10.3788/COL201816.060602.

Fiber laser sensors have attracted great interest due to their advantages of compact size, high sensitivity, large dynamic range, and real-time detection. A fiber laser can be classified into several types based on different structures of the resonant cavity, such as the distributed feedback (DFB) fiber laser[1], distributed Bragg reflector (DBR) fiber laser[2], and fiber ring cavity laser[3]. In the past few years, a great number of reports about fiber laser acoustic sensors have been proposed. Kersey *et al.*[4] first demonstrated DFB fiber laser hydrophones in 1994. Zhang *et al.*[5] presented a DFB fiber laser hydrophone with enhanced sensitivity based on double diaphragms. Lyu *et al.*[6] demonstrated the ability of the DBR fiber laser sensor in dual-frequency ultrasound measurement. Meanwhile, fiber laser sensors for magnetic field detection have been studied over the years. According to the measurement principle, they can be divided into different types. Cheng *et al.*[7] proposed a DBR fiber laser sensor for magnetic field detection based on the Faraday effect. Cranch *et al.*[8] reported a DFB fiber laser magnetic field sensor based on Ampere's force, which can achieve high magnetic resolution of 5 nT. He *et al.*[9] proposed a magnetic field sensor based on a dual-polarization DBR fiber laser with doped Terfenol-D particles. Bai *et al.*[10] proposed a fiber ring cavity laser magnetic sensor based on magnetic fluid (MF) with a magnetic field sensing sensitivity of 1.2 pm/mT.

Generally, fiber laser sensors for simultaneous measurements are rarely reported. Yin *et al.*[11] proposed a dual-wavelength fiber ring laser sensor based on a multimode fiber (MMF) polarization maintaining fiber Bragg grating (PMFBG) filter for simultaneous axial strain, temperature, and refractive index (RI) sensing. Wang *et al.*[12] reported an optoelectronic hybrid DFB fiber laser sensor for simultaneous measurement of acoustic and static

magnetic fields. The static magnetic field signal is carried by Lorentz force. However, an AC is necessary.

Acoustics and magnetism have a wide range of applications, especially under water. For seabed earthquake monitoring, the motions of the ocean floor are always accompanied by acoustic and magnetic anomalies. For a submarine, it needs magnetometers for geomagnetic navigation and hydrophones to avoid obstacles.

In this Letter, we present a novel DFB fiber laser sensor based on the giant magnetostrictive material Terfenol-D $(Tb_{0.3}Dy_{0.7}Fe_{1.92})$. The acoustic pressure can directly act on the surface of the fiber laser, and the longitudinal strain of the magnetostrictive materials induced by magnetic fields can be transferred to the fiber laser. Both the acoustic and magnetic signals can be demodulated in the frequency domain. Compared to the sensors mentioned above, this sensor is a fit for long-time monitoring, insensitive to temperature variation, and has a compact size. Thus, this sensor is very promising in underwater detection and ocean bottom observation.

The proposed fiber laser sensor is shown in Fig. 1. To eliminate the effect of the magnetic field, all of the components are made of a non-magnetic aluminum alloy. The designed metal structure is a circular cylindrical shell, which is partly hollowed out, and can be evenly divided into four sections along its circumference. Therefore, acoustic pressure can couple inside the sensor shell through the sensing holes and act on the fiber laser. The Terfenol-D tube is in a size of $\Phi 10$ mm $\times 10$ mm and is hollow in the center (provided by Huizhou South Rare Earth Functional Material Institute Co.). A pre-stressed fiber laser is fixed at the middle of the cover and the Terfenol-D tube. The polyurethane tube is used for temperature compensation.
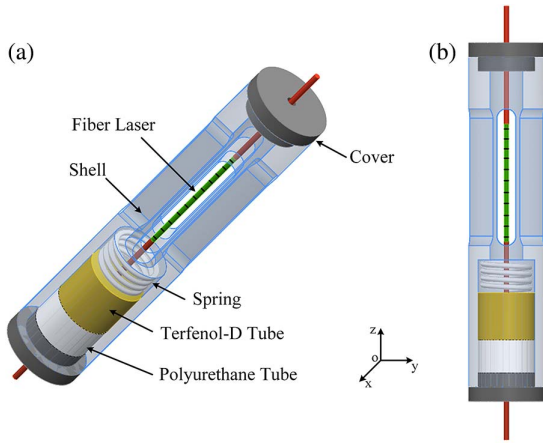
Fig. 1. (a) Schematic view of the designed fiber acoustic and magnetic sensor and (b) its front view.

In general, vibrating wire sensors (VWSs) have been implemented in numerous ways and applied in various areas, including structure health monitoring, civil engineering, and geotechnical engineering. The underlying principle of VWS is that vibrating strings help with measuring relative displacements in a mechanical system[13]. Since the resonant frequency of a string increases when it is stretched and decreases when it is shortened, monitoring the resonant frequency yields the current length of the string.

In this Letter, the fiber laser is regarded as a vibrating wire, and a sweeping acoustic signal is applied. The fiber laser will start resonating when the frequency of the acoustic signal is at the resonant frequency of the fiber laser. Meanwhile, when an external magnetic field is applied, the Terfenol-D tube will exhibit longitudinal extension, resulting in the length change of the fiber laser, which will lead to the change of resonant frequency of the fiber laser.

For the measurement of the static magnetic field, as is mentioned above, the fiber laser is regarded as a vibrating wire. Its free vibration equation can be expressed as

$$\frac{\partial_y^2}{\partial t^z} - \frac{T}{\delta}\frac{\partial^2 y}{\partial x^2} = 0, \tag{1}$$

where T is the tension of the fiber laser, δ is the linear density of the fiber laser, and t is time.

When the acoustic signal acts on the fiber laser, it will begin to vibrate and form a standing wave, which can be expressed as the following:

$$y = B\sin\frac{n\pi}{C}x\sin\left(\frac{n\pi}{l}\sqrt{\frac{T}{\delta}}t + \Phi\right), \tag{2}$$

where B is the amplitude of vibration, n is the mode of vibration, l is the length of fiber laser, and Φ is the initial phase of vibration.

Thus, the resonant frequency ($n = 1$) of the fiber laser can be expressed as

$$f_0 = \frac{1}{2l_0}\sqrt{\frac{\sigma}{\rho}} = \frac{1}{2l_0}\sqrt{\frac{E\varepsilon_0}{\rho}} = \frac{1}{2l_0}\sqrt{\frac{E\Delta l}{\rho l_0}}, \tag{3}$$

where ρ is the density of the fiber laser, l_0 is the initial length of the fiber laser, and Δl is the change of the length of the fiber laser. E is Young's modulus of the fiber laser, and ε_0 is the initial strain of the fiber laser.

When an external magnetic field is applied to the sensor, the Terfenol-D material exhibits longitudinal extension, which will cause changes in the strain of the fiber laser. The relationship between the strain of Terfenol-D material ε and external magnetic field H is given by[14]

$$\varepsilon = \frac{\Delta L}{L} = C_f H^2, \tag{4}$$

where L is the length of the Terfenol-D material. ΔL is the change of length of the Terfenol-D material. Ideally, $\Delta l = \Delta L$. C_f is the magnetostrictive coefficient of the Terfenol-D material.

Meanwhile, the temperature variation will also cause changes in the strain of the fiber laser. Thus, when temperature and magnetic field change simultaneously, the resonant frequency of the fiber laser can be expressed as

$$f_x^2 = \frac{1}{4l_x^2}\frac{\sigma}{\rho} = \frac{1}{4l_x^3}\frac{E\Delta l}{\rho} = \frac{E}{4l_x^2}\frac{C_f H^2 L + \partial_1 l_1 + \partial_2 l_2 + \partial_3 l_3}{\rho}, \tag{5}$$

where ∂_1 is the thermal expansion coefficient of the shell, and $\partial_1 = 20 \times 10^{-6}\,°\text{C}^{-1}$. l_1 is the length of the shell, which is 70 mm. ∂_2 is the thermal expansion coefficient of the Terfenol-D tube, and $\partial_2 = 12 \times 10^{-6}\,°\text{C}^{-1}$. l_2 is the length of the Terfenol-D tube, which is 10 mm. ∂_3 is the thermal expansion coefficient of the polyurethane tube, and $\partial_3 = 180 \times 10^{-6}\,°\text{C}^{-1}$. l_3 is the length of the polyurethane tube, which is 7 mm. l_x is the length of the fiber laser. Approximately, $l_x = l_0$.

When the temperature changes, the shell will vary in the opposite direction with the Terfenol-D and polyurethane tube. It can be obtained that $\partial_1 l_1 + \partial_2 l_2 + \partial_3 l_3 \approx 0$ after calculation. So, this sensor is able to achieve temperature self-compensation.

Thus, according to Eq. (5), the relationship between the resonant frequency of the fiber laser and the external magnetic field can be expressed as

$$f_x = \sqrt{\frac{C_f E L}{4l_0^3 \rho}}H. \tag{6}$$

According to Eq. (6), the resonant frequency changes linearly with the external magnetic field, and the length of the fiber laser and Terfenol-D tube will affect the magnetic field sensitivity of this sensor.

For the measurement of acoustic pressure, it can be calculated by measuring the phase shift of the fiber laser. To accurately measure the local pressure of the fiber laser

sensor, a standard piezoelectric acoustic sensor is put close to it. Hence, the sensitivity of this sensor M_J can be expressed as

$$M_J = \frac{\Delta\varphi}{U} M_s, \tag{7}$$

where M_s is the sensitivity of the standard piezoelectric acoustic sensor. $\Delta\varphi$ is the phase shift of the fiber laser sensor. U is the output voltage of the standard piezoelectric acoustic sensor.

The experiment setup is shown in Fig. 2. A magnetic field generator based on Helmholtz coils produces a static uniform magnetic field. There are two sensors placed in the uniform region of the Helmholtz coil. The red one represents the optic fiber magnetic field sensor, and the yellow one represents the standard piezoelectric acoustic sensor (BK4189), which is used as a reference because the frequency response of the speaker is not flat. The two speakers are placed 50 cm away from the sensor. Speaker 1, controlled by function generator 1, is used to produce a sweeping sinusoidal acoustic signal; the fiber laser will reach its maximum vibration amplitude when the frequency of the acoustic signal is close to the resonant frequency of the fiber laser. Speaker 2, controlled by function

generator 2, is used to produce a single acoustic signal. Both of these acoustic signals can be well distinguished in the frequency domain. The amplitude and frequency of the acoustic pressure are adjustable. The fiber laser demodulator consists of a 980 nm pumping light source and several fiber optic devices, such as isolators, fiber coupler, wavelength division multiplexers (WDMs), photoelectric detectors, an unbalanced Mach–Zehnder fiber interferometer, and a data acquisition system (DAQ). The interrogation of this sensor can be achieved by phase-generated carrier (PGC) demodulation[15]. The demodulation results can be displayed through the computer both in the time domain and frequency domain.

In this experiment, we use function generator 1 to apply a sweep sinusoidal signal to speaker 1 from 20 Hz to 2 kHz, and the sweep speed is 1 Hz/s. When the frequency of the acoustic signal is 360 Hz, we observe that the fiber laser sensor reaches its maximum response after being calibrated by the standard piezoelectric acoustic sensor. Therefore, the resonant frequency of this sensor is 360 Hz. When an external magnetic field is applied, we find that the resonant frequency of this sensor changes. Meanwhile, we use speaker 2 to apply a single acoustic signal, which will act on the surface of the fiber laser and causes a phase shift of the fiber laser.

Figure 3 shows the demodulation result of the sensor in the frequency domain. As shown in Fig. 3(a), the red curve represents the response of the sensor at its resonant frequency at 360 Hz and at another 1 kHz acoustic signal. The blue curve presents the response when an external magnetic field of 30 mT is applied. It is obvious that the resonant frequency decreases when the magnetic field exists. What is more, the red curve is almost covered by the blue curve at 1 kHz, which means that the two acoustic signals do not affect each other no matter whether the magnetic field is applied. In Fig. 3(b), the red curve represents the response of the sensor at its resonant frequency at 360 Hz and at another 1 kHz acoustic signal, and the blue curve represents the response of the sensor at its resonant frequency at 360 Hz and at another 800 Hz acoustic signal. It shows that the red curve is almost covered by the blue curve at 360 Hz, because the resonant frequency does not move when the acoustic signal changes.
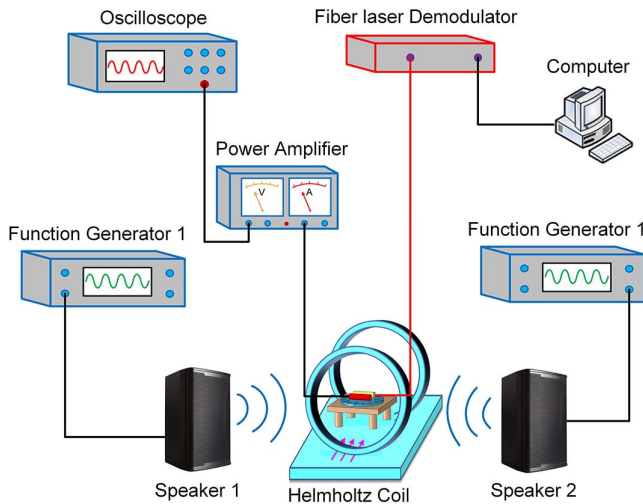

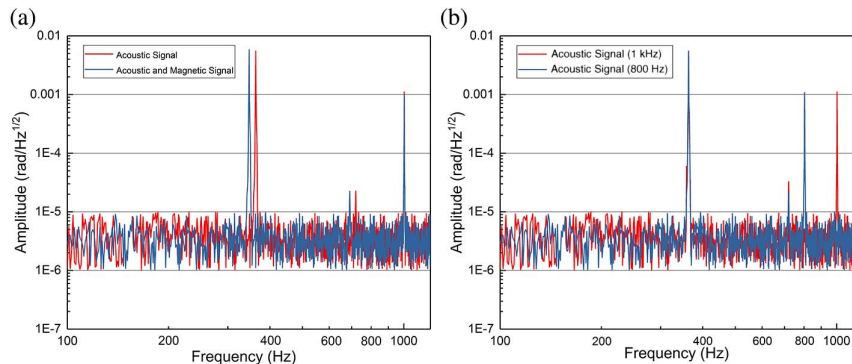Fig. 2. Schematic of the test system.

Fig. 3. Simultaneous acoustic and magnetic signals in the frequency domain.

In Fig. 3, it also shows that the noise floor of the magnetic sensor is lower than 1×10^{-5} rad/Hz$^{1/2}$. When the acoustic signal is applied, the responding amplitude of the sensor is over 20 dB. Despite environment noises at a few frequency points, the responding mixed signal of the magnetic field achieves a good signal-to-noise ratio (SNR).

In this experiment, the acoustic pressure sensitivity of this sensor is tested. Figure 4 shows the frequency response of this sensor within 1 kHz after being calibrated by the standard piezoelectric acoustic sensor. The discrete testing points with the interval of a 1/3 octave are connected by modified Bezier fitting. As shown in Fig. 4, the frequency response varies across the measured bandwidth with a maximum sensitivity between 315 and 400 Hz because the resonant frequency of the fiber laser is 360 Hz. It also shows that the frequency response curve from 100 to 250 Hz is relatively flat, and the average acoustic pressure sensitivity within this range is −130 dB (0 dB re 1 rad/μPa).

The relationship between the fiber laser resonant frequency and magnetic field is shown in Fig. 5(a). The initial resonant frequency is located at 360 Hz, and it gradually shifted toward a lower frequency as the strength of the magnetic field increased. The applied static external magnetic field is from 0 to 50 mT, and the step length is 5 mT. The red curve in the figure is the linear fitting curve of the measured data, which keeps a good linearity. Therefore, the magnetic field sensitivity is 0.57 Hz/mT with an adjusted R-squared value of about 0.997. Currently, the frequency resolution of this demodulation system is 1 Hz, so the magnetic field resolution of this sensor can be calculated as 1.75 mT.

Figure 5(b) shows the directivity of this sensor. The test is implemented by putting the senor on a rotating stage at the center of the Helmholtz coil and rotating it from 0° to 360° in a step of 30° (0° means the Terfenol-D tube is parallel to the magnetic field). The magnitude of magnetic field is set at 50 mT. As shown in Fig. 5(b), the discrete testing points are connected by modified Bezier fitting. The sensor reaches its maximum response at 0 dB when Terfenol-D tube is parallel to the direction of the magnetic field. It also shows that the sensor exhibits its minimum response when the Terfenol-D tube is perpendicular to the magnetic field. The cross sensitivities at 90° and 270° are −23.1 and −20.6 dB, respectively. However, the imperfect symmetry exists, which may result from the hysteresis effect of the Terfenol-D material. In addition, the errors of the rotating stage cannot be ignored.

In conclusion, we demonstrate a novel optical fiber sensor for simultaneous measurement of acoustic and magnetic fields by using a DFB fiber laser and Terfenol-D material within a miniature package with dimensions of Φ12 mm × 85 mm. The external magnetic field can be monitored by detecting the variation of the resonant frequency of the fiber laser, which can be measured when there is a wide-band acoustic signal or seismic signal. An experiment of this sensor is carried out, and the testing results show that simultaneous measurement of acoustic pressure and static magnetic field can be achieved. It also shows that the detections of the acoustic and magnetic fields have little effect on each other in the dynamic range. Meanwhile, this sensor is insensitive to temperature changes for the use of the polyurethane material to compensate the temperature effect. The tested acoustic pressure sensitivity is about −130 dB (0 dB re 1 rad/μPa). This sensor demonstrates a good linearity with a magnetic field sensitivity of 0.57 Hz/mT. This sensor also presents orientation dependence of magnetostriction, which has a potential to be fabricated as a tri-axial sensor. So, this sensor is expected to be used in underwater object detection and ocean bottom observation.
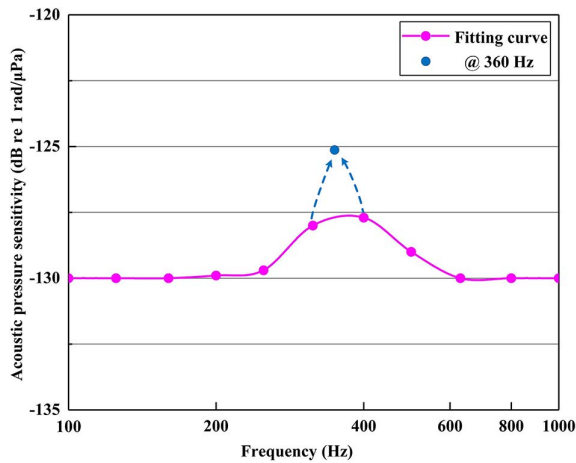

Fig. 4. Acoustic frequency response of the sensor.
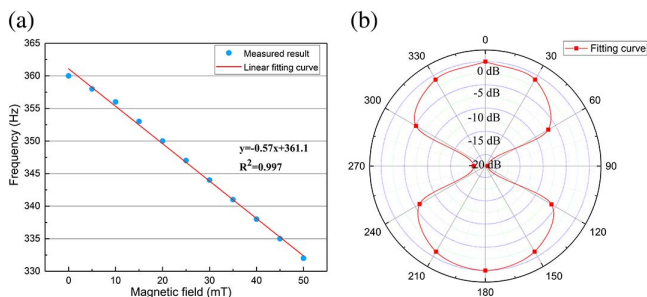

Fig. 5. (a) Measured resonant frequency shift of the fiber laser for various applied magnetic field magnitudes. (b) Directivity of this sensor.

References

1. Y. Tan, Y. Song, W. T. Zhang, and F. Li, Chin. Opt. Lett. **14**, 120602 (2016).
2. B. W. Pan, L. Q. Yu, L. Guo, L. M. Zhang, D. Lu, X. Chen, Y. Wu, C. Y. Lou, and L. J. Zhao, Chin. Opt. Lett. **14**, 030604 (2016).

3. J. Zhang, Z. Y. Kong, Y. Z. Liu, A. M. Wang, and Z. G. Zhang, Photon. Res. **4**, 29 (2016).

4. A. D. Kersey, K. P. Koo, and M. A. Davis, Proc. SPIE **2292**, 112 (1994).

5. W. T. Zhang, Y. L. Liu, F. Li, and X. Hao, J. Lightwave Technol. **26**, 1352 (2008).

6. K. Vivek, R. Rajesh, C. V. Sreehari, K. S. Sham, K. Shajahan, T. V. Praveen, T. Santhanakrishnan, and K. P. B. Moosad, J. Lightwave Technol. **35**, 4097 (2017).

7. L. H. Cheng, J. L. Han, L. Jin, Z. Z. Guo, and B. O. Guan, Opt. Express **21**, 30162 (2013).

8. G. A. Cranch, G. M. H. Flockhart, and C. K. Kirkendall, Meas. Sci. Technol. **20**, 034023 (2009).

9. W. He, L. H. Cheng, Q. Yuan, Y. Z. Liang, L. Jin, and B. O. Guan, Chin. Opt. Lett. **13**, 050602 (2015).

10. X. K. Bai, J. Yuan, J. Gu, S. F. Wang, Y. H. Zhao, S. L. Pu, and X. L. Zeng, IEEE Photon. Technol. Lett. **28**, 118 (2015).

11. B. Yin, M. G. Wang, S. H. Wu, Y. Tang, S. C. Feng, Y. Wu, and H. W. Zhang, Opt. Express **25**, 30955 (2017).

12. Z. G. Wang, W. T. Zhang, W. Z. Huang, S. W. Feng, and F. Li, Opt. Express **23**, 24389 (2015).

13. F. Bourquin and M. Joly, Smart Mater. Struct. **14**, 247 (2004).

14. K. Rick and A. Flatau, J. Intell. Mater. Syst. Struct. **15**, 128 (2004).

15. G. S. Fang, T. W. Xu, and F. Li. IEEE Photon. Technol. Lett. **25**, 2188 (2013).